Cement and Concrete Research 39 (2009) 116–125

Contents lists available at ScienceDirect

Cement and Concrete Research

journal homepage: http://ees.elsevier.com/CEMCON/default.asp

Chloride-induced corrosion products of steel in cracked-concrete subjected to different loading conditions

Shahzma J. Jaffer *, Carolyn M. Hansson

Department of Mechanical and Mechatronics Engineering, University of Waterloo, 200 University Ave West, Waterloo, ON, Canada N2L 3G1

ARTICLE INFO

Article history:
Received 1 April 2008
Accepted 6 November 2008

Keywords:
Crack
SEM (B)
Corrosion (C)
Chloride (D)
Concrete (E)

ABSTRACT

This project focused on examining the composition and distribution of chloride-induced corrosion products at the rebar–concrete interfaces and on crack surfaces in reinforced ordinary Portland cement concrete (OPCC) and high performance concrete (HPC) subjected to different loading conditions. The results indicated that, regardless of the type of loading, there was a larger distribution of corrosion products along the rebar surface in the HPC than in the OPCC. Also, dynamic loading caused a greater detachment of the aggregate–paste bond in OPCC than static loading. The opening and closing of the cracks in salt solution under dynamic load forced corrosion products to flow from the rebar–concrete interface into the cracks in both OPCC and HPC. As a result, corrosion products diffused from the crack into the cement paste in the dynamically loaded OPCC but remained in the cracks in the dynamically loaded HPC, where they induced branched cracks. The mill-scale on the rebar was also evaluated before and after being embedded in concrete and was observed to be porous allowing ingress of species from the cement paste.

1. Introduction

Corrosion of steel bars (rebar) affects the durability of reinforced concrete in two ways: (i) it reduces the cross-section of the rebar, thereby, decreasing its load bearing capacity and (ii) it degrades the integrity of the surrounding concrete. As illustrated in Fig. 1 [1], corrosion products of iron are expansive and their formation can cause cracking in the concrete. Nevertheless, very few studies have actually examined the effect of corrosion on cracking in concrete. Cabrera [2] observed that corrosion caused cracks parallel to the reinforcement when the reinforcement was corroded using an impressed current. Andrade et al. [3] found that only a few micrometers of rebar corrosion induced visible cracks (~0.1 mm width) in reinforced concrete also corroded with an impressed current. However, studies that use impressed currents to cause corrosion of the steel in concrete are not realistic representations of what happens in actual concrete structures where chloride ions are the predominant cause of corrosion [4,5].

Some researchers have also tried to examine the effect of corrosion on cracking by means of simulation. Allan [6] applied hydraulic pressure through reinforcing bars containing pre-drilled internal passageways to simulate the cracking of concrete from localized formation of corrosion products. Uddin et al. [7] also relied on hydrostatic pressures from expansive agents to simulate cracks in reinforced concrete. They claim that cracks in concrete propagate by mode I fracture (opening mode) with small contributions from mixed mode and mode II fracture (in-plane shear). Ohtsu and Yosimura [8] modelled crack initiation and crack propagation in concrete due to reinforcement corrosion, taking into account various types of cracks (surface, spalling, internal vertical and diagonal cracks). Their conclusions identify the conditions under which the different types of cracks form and propagate.

All the studies listed above assume that corrosion products accumulate at the rebar–concrete interface and that cracking is initiated from this interface because of pressure from the corrosion products. Although she made the same assumption, Allan [6], did consider the possibility of corrosion products diffusing into the concrete without cracking it. She suggested that the time to cracking in concrete may be extended if the concrete is porous and contains voids which can act as storage sites for corrosion products.

It is important to note that concrete always contains cracks and that those cracks formed prior to initiation of reinforcement corrosion, have an immense impact on the corrosion of rebar. Studies [9,10] have shown that, in cracked reinforced concretes exposed to chlorides, corrosion occurred on the rebar only where it was intercepted by cracks in the concrete while the rebar in the uncracked regions was passive.

The examination of chloride-induced corrosion products of steel in concrete has been a recent development. Hence, literature in this area is limited. For reinforced concrete containing carbon steel and exposed to marine environments for five years, Suda et al. [11] detected magnetite, goethite and lepidocrocite. Aligizaki et al. [12] observed that corrosion products could diffuse into the aggregate–paste interface in concrete and that, at the interface, the corrosion product adjacent to the aggregate was magnetite while that close to cement paste was hæmatite. Marcotte and Hansson [13] observed that

* Corresponding author. Tel.: +1 519 888 4567x32319; fax: +1 519 885 5862.
E-mail address: sjaffera@engmail.uwaterloo.ca (S.J. Jaffer).

0008-8846/$ – see front matter © 2008 Elsevier Ltd. All rights reserved.
doi:10.1016/j.cemconres.2008.11.001

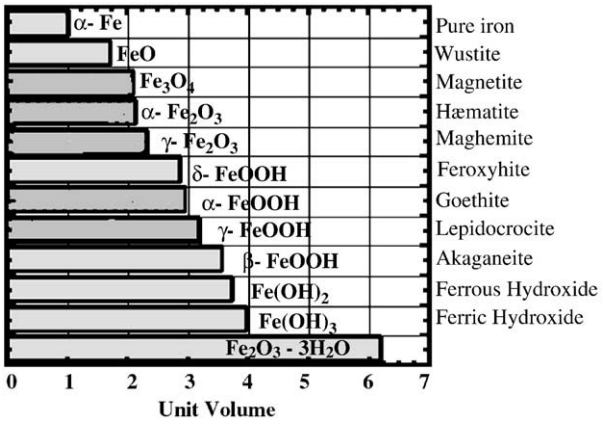

Fig. 1. Corrosion products of iron [1].

corrosion products were distributed in the concrete up to 5 mm from the rebar in high performance concrete (HPC) without silica fume while, in HPC with silica fume, the corrosion products were concentrated in the cracks in concrete intersecting the steel. This difference was attributed to the less porous structure of HPC with silica fume and its superior bonding to the rebar. This conclusion was supported by the observation that akaganeite and goethite, which are more oxidized and expansive forms of iron corrosion products, were found in the former while the latter contained only magnetite. These authors [14] also compared the corrosion products of steel in cracked ordinary Portland cement concrete (OPCC) (w/cm=0.41) with those in cracked HPC (w/cm=0.27). They detected maghemite in the OPCC which was not found in the HPC suggesting that less oxygen was available in the OPCC. The absence of maghemite was attributed to cracks present in HPC which enabled corrosion products to move away from the steel–concrete interface where the oxygen supply was considered to be higher and resulted in the formation of akaganeite and goethite.

The most expansive corrosion product detected to date in reinforced concrete is akaganeite, which is about 3.5 times the original volume of iron. Akaganeite was observed by Marcotte and Hansson [13,14] in cracked concrete that was statically loaded i.e. experienced constant load over time. However, reinforced concrete structures such as bridge decks and parking garage slabs experience variably (dynamic) loading over time due to the flow of traffic. This could affect the microstructure of concrete thereby influencing (a) the corrosion products formed in the reinforced concrete and (b) the distribution of these products in the concrete.

Consequently, the objectives of this research were to examine the distribution and identity of corrosion products formed in statically and dynamically loaded cracked reinforced concretes. Since reinforcing steel is used in its as-rolled condition with its mill-scale intact, the mill-scale on the rebar was also evaluated before and after being embedded in concrete.

2. Experimental procedure

2.1. Specimen preparation

Reinforced concrete beams were made with OPCC (w/cm=0.46) and HPC (w/cm=0.35) using the mixture proportions given in Table 1. Each beam contained two 10 M (11.3 mm in diameter) carbon steel reinforcing bars positioned equidistant from each other and from the surfaces of the concrete beams. The beams had a 120 mm×70 mm cross-section and a height of 1200 mm. Immediately after casting, both types of beams were cured under wet burlap and plastic sheet. The OPCC beams were cured for two days and the HPC beams were subjected to curing for seven days as per the Ministry of Transportation of Ontario requirements [15].

Table 1
Mixture proportions for OPCC and HPC

Component	OPCC	HPC
Type 10 Portland cement, kg	355	0
Type 10ESF (containing 8% Silica fume), 1kg	0	337
Ground granulated blast furnace slag, kg	0	113
Sand, kg	770	718
Stone, <12.5 mm, kg	1070	1065
Water, l	165	158
Air entrainer	40 ml/100 kg of cementitious material	65 ml/100 kg of cementitious material
Water reducer	250 ml/100 kg of cementitious material	250 ml/100 kg of cementitious material
Superplasticizer		635 ml–1271 ml/100 kg cementitious material
w/cm ratio	0.46	0.35
Compressive strength tests (performed 27 months after casting), Mpa	42.7	62.5

All the beams were pre-cracked at their midsection in three-point bending by coupling them in pairs, as illustrated in Fig. 2, and subjected to either static or cyclic (dynamic) loading conditions. Static loading was applied to four pairs of beams by tightening the nuts on the threaded rods at the top end of each pair of beams (Fig. 2) to maintain a deflection of 3 mm. The loading set up allowed the same load to be applied at the bottom end. Dynamic loading was also applied to four pairs of beams using air cylinders and pistons, which were connected to an air supply and controlled by a square wave generator. The load applied at the top end of each pair of the beams caused the same deflection as in the statically loaded beams and was applied at a frequency of 0.5 Hz for 1–2.5 h a day.

The loaded beams were placed upright in tubs and subjected to four week cycles. During the first two weeks, the beams were immersed in 3% chloride (as sodium chloride) solution to just above the crack level at their mid-point. For the second two weeks, the beams were left in ambient laboratory conditions to dry. This exposure developed three regions on each beam where corrosion measurements were performed: (a) non-submerged, (b) submerged uncracked and (c) submerged cracked. The results of these measurements have been presented in [9]. The period of time between casting the beams and loading was about six months. They were exposed to chloride solution immediately after loading.

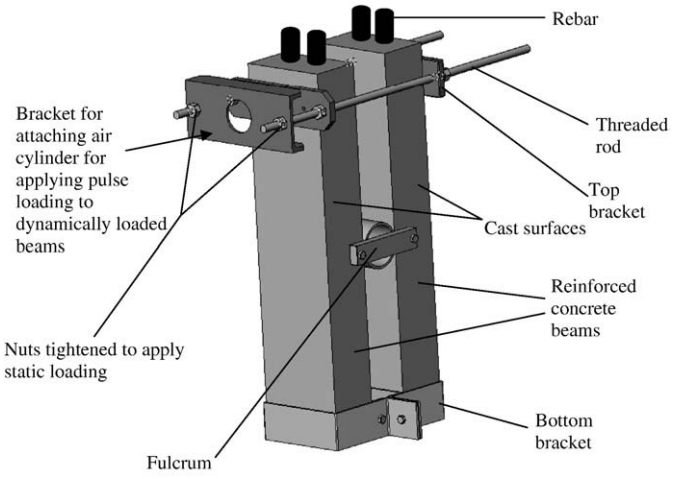

Fig. 2. Set up for applying static and dynamic loading to the beams.

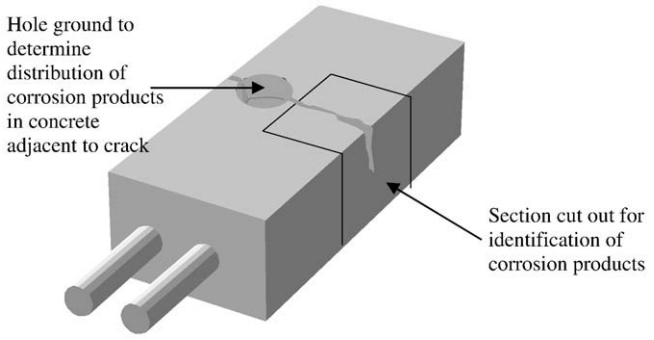

Fig. 3. Showing the locations of the ground hole and the segment used for analysis of corrosion products.

2.2. Distribution and identification of corrosion products

The distribution of corrosion products at loading cracks in the concrete was examined in three sections: (i) in sections parallel to the exposed tensile surface and perpendicular to the crack; (ii) on the surface of the crack and (iii) along the surface of the rebar. To observe the crack in a section perpendicular to its length, a hole was ground into the concrete at the central crack over one of the rebars (Fig. 3) after nine months of exposure to salt solution (fifteen months after casting) using an 8 mm diameter diamond grinding bit which rotated over an area of 70 mm. This hole was ground in increments of 2 or 3 mm in two beams of each concrete type subjected to static and dynamic loading and, at every grinding step, the concrete and crack were photographed. Due to the limitations of the grinding equipment, the maximum depth of the holes was 21 mm which was 9 mm from the rebar surface. Hence, the distribution of corrosion products at the rebar–concrete interface was not examined in this aspect of the investigation.

The corrosion products on the surface of the rebar and on the concrete walls of the crack were analysed as follows. Segments of the concrete with the rebar intact were cut out of the beam at the mid-section cracks as illustrated in Fig. 3 and were introduced in a glove box containing an inert atmosphere (nitrogen). Inside the glove box, concrete was detached from the steel, which was placed in an airtight chamber containing an optically flat glass window. The chamber was sealed before being taken out of the glove box while the concrete was left in the glove box with the crack surfaces still intact (Fig. 4(a)). The chamber containing the steel was then taken to the Raman spectrometer for analysis in situ. After analysis of the steel, the chamber was reintroduced inside the glove box and the steel was removed. The crack surfaces (Fig. 4(b)) of the concrete were opened and placed inside the chamber before it was sealed again and taken out of the glove box for analysis.

Raman spectroscopy was conducted using a Renishaw RM 1000 system. This system included an Olympus optical microscope, a Peltier-cooled charge couple device (CCD) detector and a spectrograph. The source used for excitation was a 35 mW HeNe laser with a wavelength of 632.8 nm; however, the power was reduced to 3 mW on the surface of the sample by the system to prevent the products from being altered by heating. The samples, inside the airtight chamber, were placed on the stage of the optical microscope and were focused under 50 times magnification using white light and photographed. The illumination was then changed to laser lighting irradiating an area 5 μm in diameter and ~3 μm in depth. This area was than scanned using five accumulations with each accumulation scanning Raman shifts from 70 cm^{-1} to 1800 cm^{-1}. The results of the accumulations were averaged by the Renishaw Wire 2.0 software. The scan produced a spectrum consisting of several peaks which corresponded to various corrosion products. A literature search was conducted to match the peaks in the spectrum to the compounds responsible for them. If more than one type of corrosion product was responsible for a particular peak in the spectrum, the peak was attributed to the compound with other peaks in the spectrum. Depending on the distribution of corrosion products, between eight and twenty 'areas' were scanned on each examined surface.

The distribution of corrosion products on the rebar at the central crack in the beams was examined by autopsying four beams of each type of concrete subjected to the different loading conditions. The beams had been exposed to the salt solution for eighteen months prior to this examination. The damage due to corrosion of the rebar surfaces has been discussed in [9] and will not be included here.

2.3. Changes in mill-scale

Mill-scale on the rebar was examined in three conditions: (i) as-received bar, i.e. not embedded in concrete, (ii) after being embedded in uncontaminated concrete for twenty-eight months and (iii) after being embedded in concrete and exposed to chlorides at a crack in the concrete for eighteen months. Small sections of the rebar (approximately 15 mm long) were mounted in a hot mounting material such that their cross-sections could be examined. They were then ground and polished to 1 μm and coated in gold to prevent charging in the electron microscope.

The sections were then observed in a JOEL JSM-6460 scanning electron microscope (SEM) under the secondary electron (SE) and backscattered electron (BSE) modes. The elemental analysis of mill-scale was obtained using an Oxford Instruments IncaX-sight energy dispersive spectroscopy (EDS) detector with an ATW2 window, which was attached to the SEM.

3. Results and discussion

3.1. Distribution of corrosion products on the rebar surface

In the OPCC regardless of the type of loading, there was a tendency for the corrosion products at the rebar–concrete interface to remain in

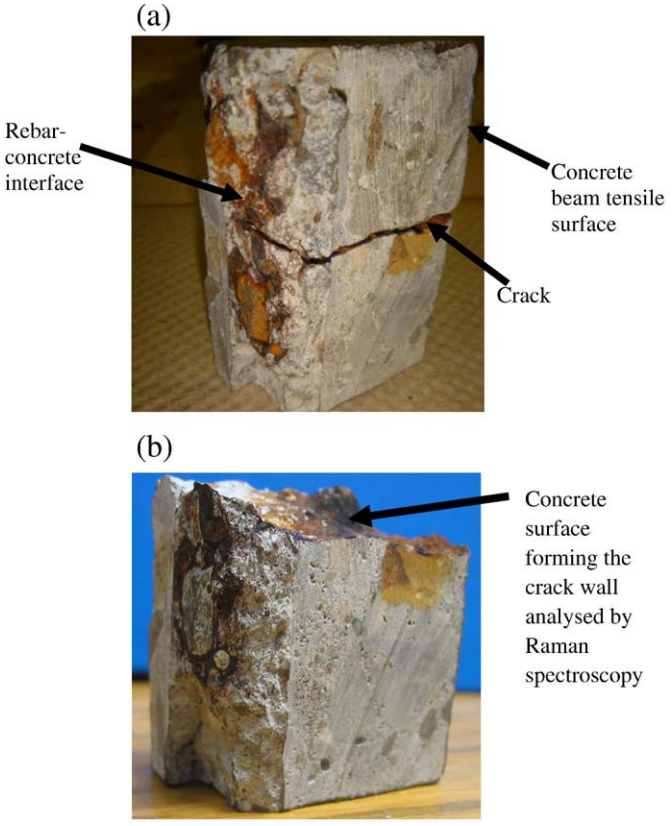

Fig. 4. Sections of concrete showing examples of (a) the intact surfaces of a crack and (b) the crack surface where corrosion products were analyzed.

Fig. 5. The distribution of corrosion products on the rebar surface at a mid-section crack in (a) OPCC and (b) HPC.

the vicinity of the crack while, in the HPC, the products tended to spread further along the rebar away from the crack. This is not as clearly evident in Fig. 5 where the length of spread on the rebar surface was about 50 mm in OPCC and about 75 mm in HPC. However, on the average, the length of spread in OPCC was 40±15 mm and in HPC it was 75±45 mm. This difference can be attributed to the variation in porosity between the two types of concretes. In both OPCC and HPC beams, the cracks bifurcated at the rebar–concrete interface and propagated parallel to the rebar along this interface; however, because OPCC was more porous than HPC, more of the corrosion products in the OPCC diffused into the concrete rather than spreading along the rebar surface. In both concretes, the corrosion products were observed only along the side of the rebar that was subjected to tensile loading. Their accumulation may have led to further de-bonding at the interface.

3.2. Distribution of corrosion products in the concrete

Examples of the morphology of the crack and corrosion products deposited in the crack in the statically loaded OPCC are shown in Fig. 6. The corrosion products diffused from the crack into the aggregate–cement paste interface can be seen in Fig. 6(b). This phenomenon may lead to detachment of the aggregate–paste bond. However, there were significantly fewer instances of this happening in the statically loaded OPCC beams than in the dynamically loaded OPCC beams. This is probably because, under dynamic loading, the loading would have opened up the interface and created free space for corrosion products to easily diffuse into. As a result, corrosion products in the statically loaded OPCC were generally confined to the crack, as shown in Fig. 6. Multi-coloured aggregates (Fig. 6(b)) were also observed at the cracks in the beams and should not be confused with corrosion products.

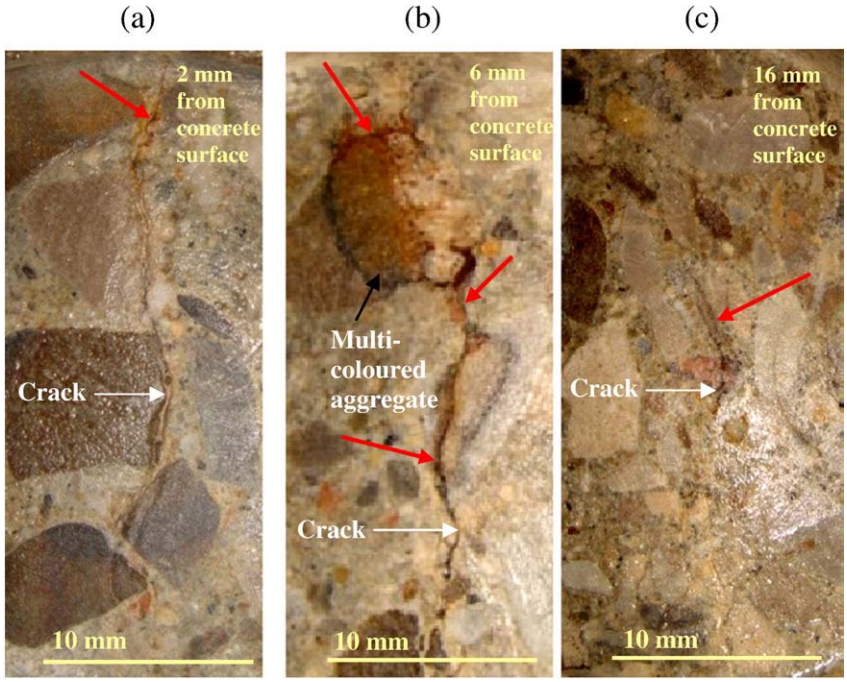

Fig. 6. Corrosion products at the central crack in the statically loaded OPCC beams. Note the multi-coloured aggregate in (b). Red arrows point to the location of visible products. Photograph (a) and (b) were obtained from the same beam and photograph (c) was obtained from a different beam. (For interpretation of the references to colour in this figure legend, the reader is referred to the web version of this article.)

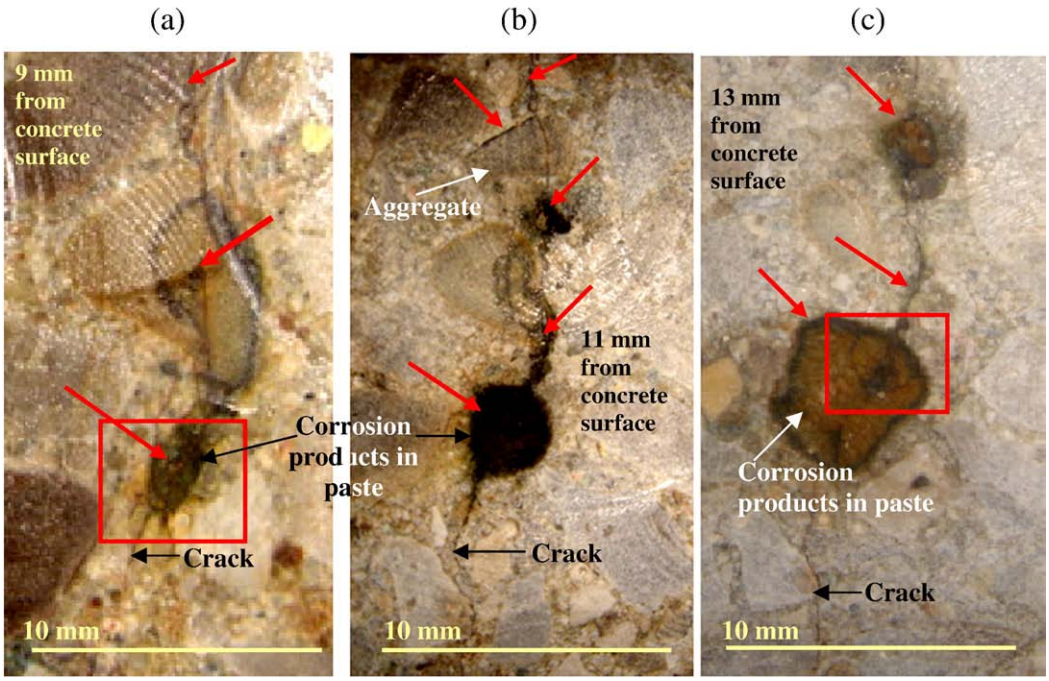

Fig. 7. Distribution of corrosion products in the dynamically loaded OPCC concretes. Red arrows point to the location of visible products. (a) 9 mm from concrete surface; (b) 11 mm from concrete surface; (c) 13 mm from concrete surface. The protruding cracks in the square regions in (a) and (c) may have been formed because of the accumulation of corrosion products. (For interpretation of the references to colour in this figure legend, the reader is referred to the web version of this article.)

In the dynamically loaded OPCC beams, the corrosion products not only diffused from the cracks into the aggregate–paste interfaces, but also into the cement paste as illustrated in Fig. 7. Where this occurred, cracking was also observed as indicated in Fig. 7(a) and (c). The accumulation of products in the crack is likely to force them to penetrate into the interconnected porosity in the cement paste. However, the products cannot move easily through the bottle-necks of the capillary pores and exert stresses on the pore walls causing the paste to crack.

In the statically loaded HPC beams, corrosion products were not observed at any depth from the concrete surface in the crack. Fig. 8 illustrates images of cracks from the statically loaded HPC concretes. The fact that corrosion products were not observed in these beams does not mean that they did not exist. As discussed above, the products in the HPC beams tended to form preferentially at the rebar–concrete interface.

In contrast, corrosion products were seen in the cracks in the dynamically loaded HPC beams as shown in Fig. 9; however, unlike those in the OPCC, they did not penetrate into the adjacent concrete. In Fig. 9(a), corrosion products can be observed inside an entrapped void, which was intersected by the crack. Fig. 9(b) and (c) show branched cracks in which the products had accumulated. Dynamically loaded HPC beams had significantly more corrosion products in the cracks than the statically loaded HPC due to the opening and closing of the cracks which allowed the salt solution to carry some of the products away from the rebar. Corrosion products tend to precipitate in the free space that is available to them. Hence, the low amount of interconnected capillary porosity in the HPC can be both an advantage and disadvantage when it comes to accommodating corrosion products. The advantage is that the products will not disperse into the concrete if empty spaces are available for them to diffuse into. However, the drawback is that, if such spaces are not available, the forces caused by the build-up of these products can cause cracking in the concrete. The corrosion products are most likely responsible for the branched cracking shown in Fig. 9(b) and (c).

The distribution of corrosion products on the crack surfaces of the central cracks in the beams subjected to the different loading conditions is illustrated in Fig. 10. In the dynamically loaded beams, the larger spread of corrosion products on the surface of the crack walls is an indication that the combination of opening and closing of the crack and salt solution was aiding this distribution.

3.3. Identification of corrosion products on the rebar surface and on the crack walls

Due to the large number of spectra obtained from each specimen of steel and concrete, the individual Raman spectra are not shown but they and their analyses can be found in [16]. Representative spectra have been illustrated in Fig. 11 and a summary of the products observed is presented in Table 2.

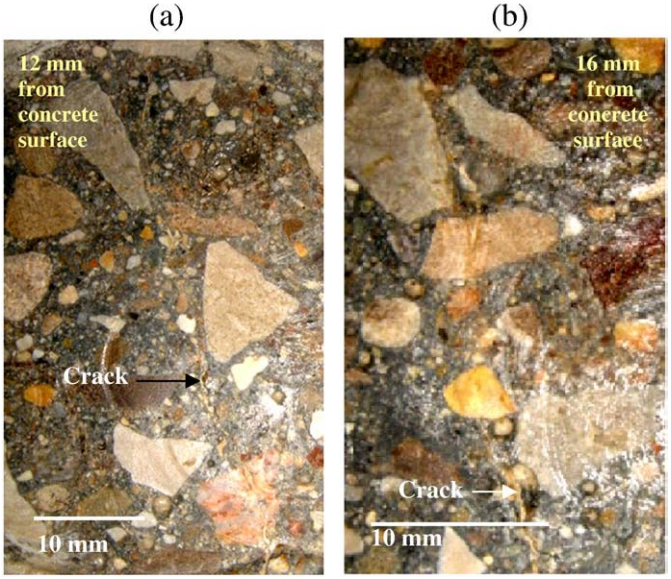

Fig. 8. Cracks in statically loaded HPC beams with no corrosion products. (a) 12 mm from concrete surface; (b) 16 mm from concrete surface.

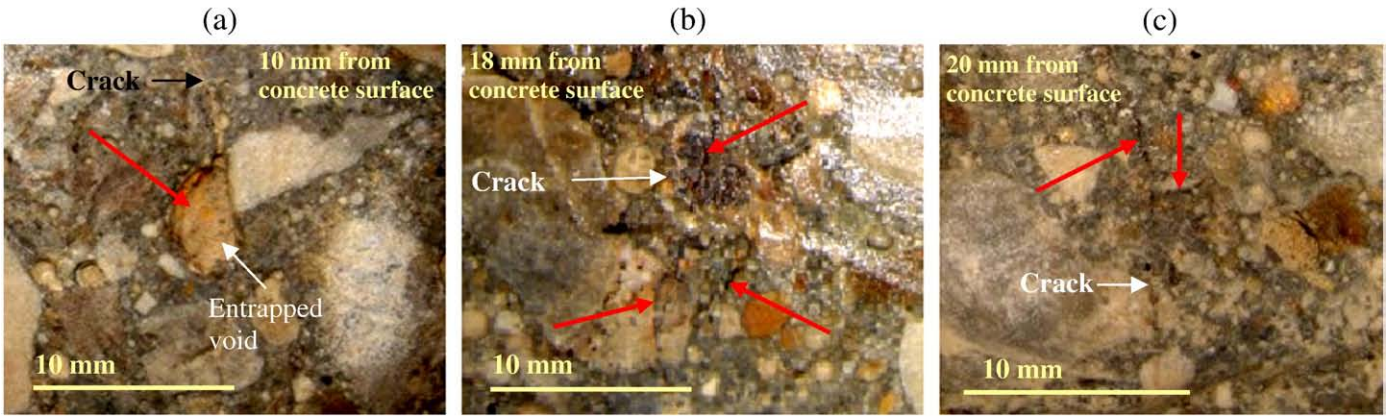

Fig. 9. Distribution of corrosion products in the dynamically loaded HPC beam. Red arrows show the location of visible corrosion products. (For interpretation of the references to colour in this figure legend, the reader is referred to the web version of this article.)

There is no discernable relationship between the products on the rebar surface and on its corresponding concrete surface. A possible reason for this is that, when corrosion products are formed, they disperse into the space available, be it in the rebar–concrete interface, in the pores of the concrete or in the crack. Unlike the situation in sound concrete, the presence of an unblocked crack allows access of air during the drying cycle and, if the crack extends to the rebar, as in this case, this provides an unlimited supply of oxygen at the rebar. This causes further oxidation of diffused products on the crack-walls and on the rebar.

The most oxidized corrosion product observed on the surface of the rebar and the concrete walls of the crack in this study was ferric hydroxide which is more voluminous than akaganeite that had been observed previously [13]. Ferric hydroxide occupies about 4 times the

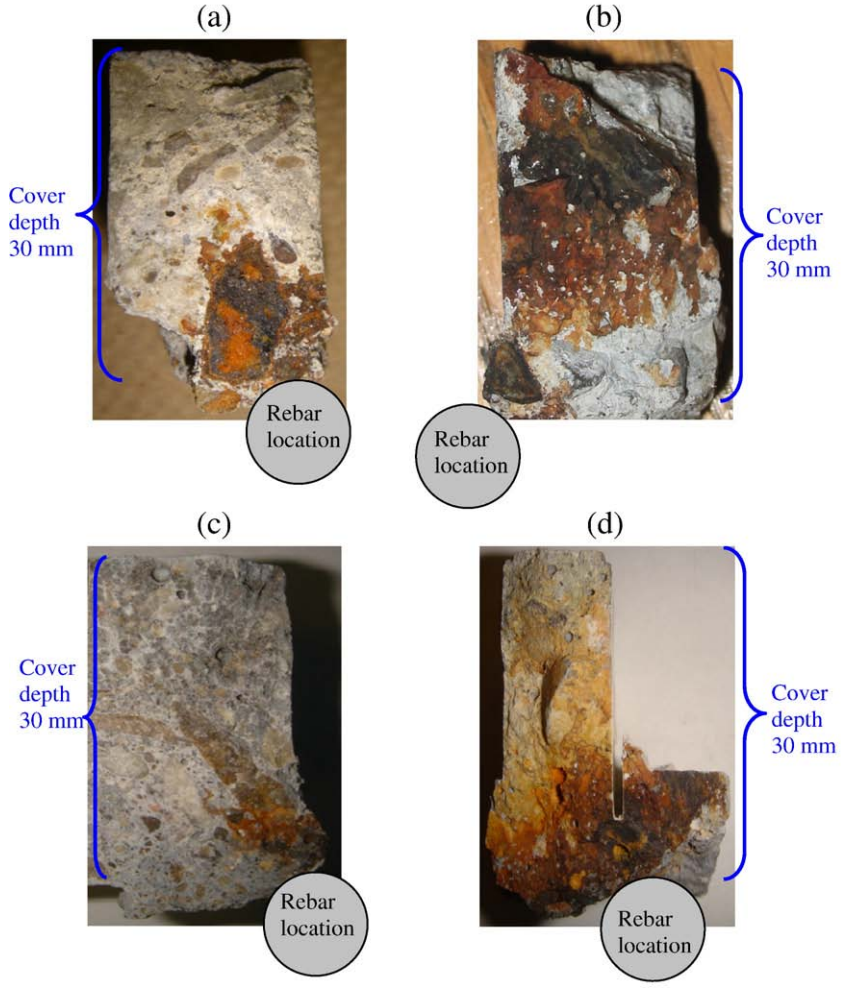

Fig. 10. Photographs showing the distribution of corrosion products on the crack-walls at the mid-section crack in (a) a statically loaded OPCC, (b) a dynamically loaded OPCC, (c) a statically loaded HPC and (d) a dynamically loaded HPC.

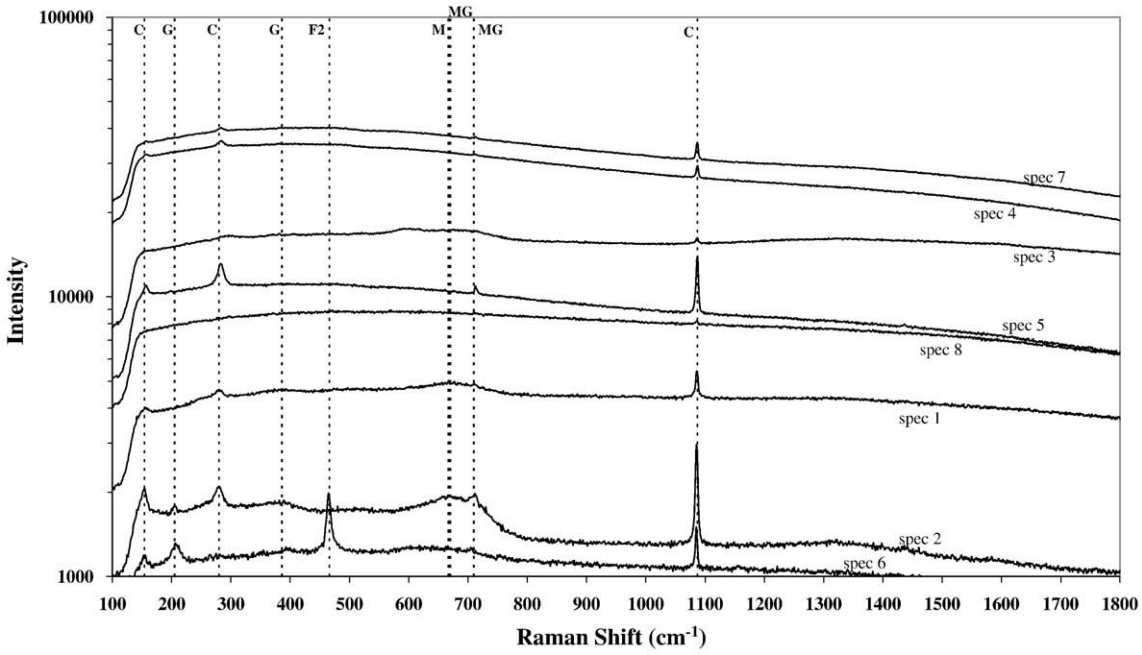

Fig. 11. Examples of spectra obtained from concrete surface. The acronyms C, G, F2, M, MG denote the calcium carbonate, goethite, ferrous hydroxide, magnetite and maghemite, respectively.

volume of iron while akaganeite occupies about 3.5 times the volume of iron [1]. However, the most important factor influencing the durability of reinforced concrete is not the *specific volume* of the corrosion products but the *amount* of each product formed, which cannot be determined.

An interesting observation was the presence of $[Fe(H_2O)_6]^{3+}$ ions (or hexaaquairon ions) on the crack-walls of the dynamically loaded OPCC. The corresponding anions could be either chloride (Cl^-) or carbonate (CO_3^{2-}) [17], which unfortunately, are not detectible by Raman spectroscopy when they are in solution. The fact that the hexaaquairon ions were detected close to the surface of the concrete as well as midway between the external concrete surface and the concrete–rebar interface implies that both water and iron ions were present in the crack at the time when Raman spectroscopy was performed. The presence of water can be explained by the high chloride concentration (sodium chloride is hygroscopic) at a crack in the dynamically loaded OPCC beams while the iron ions may have been washed into the crack by the concurrent influence of dynamic loading and the salt solution.

Hæmatite, which was observed at the rebar–concrete interface in all the concretes, was not seen on the walls of the cracks; however, magnetite, which is a less oxidized corrosion product, was evident in nearly all the concretes. The hæmatite observed at the rebar–concrete interface was probably from the existing mill-scale on the surface of the rebar; however, the magnetite was presumably a product of chloride-induced corrosion.

There was no particular order to the spatial distribution of corrosion products on the concrete surfaces. Magnetite and maghemite were observed at locations close to the rebar as well as close to the external surface of the beam in the dynamically loaded concretes. This spread could be caused by the opening and closing of the crack in the salt solution. Magnetite and maghemite were also seen wherever corrosion products were observed in the statically loaded concretes. The FeOOH compounds (e.g. akaganeite, goethite and feroxyhite), ferrous and ferric hydroxide were found in the vicinity of, or intermingled, with magnetite and maghemite. These expansive compounds could have been formed when magnetite or maghemite reacted with the salt solution.

Table 2
Corrosion products in the concrete beams

Beam	Corrosion products on rebar at a macro-crack	Corrosion products on the macro-crack walls in concrete
Statically loaded OPCC	Hæmatite[a]	Magnetite
	Maghemite	Maghemite
	Goethite	Lepidocrocite
	Ferric hydroxide	Ferric hydroxide
Dynamically loaded OPCC	Hæmatite[a]	$[Fe(H_2O)_6]^{3+}$
	Feroxyhite	Magnetite
	Lepidocrocite	Maghemite
	Ferric hydroxide	Akaganeite
Statically loaded HPC	Hæmatite[a]	Magnetite
	Maghemite	Maghemite
	Feroxyhite	Goethite
	Goethite	Ferrous hydroxide
	Lepidocrocite	
	Akaganeite	
	Ferric hydroxide	
Dynamically loaded HPC	Magnetite[a]	Maghemite
	Hæmatite[a]	Feroxyhite
	Maghemite	Goethite
	Feroxyhite	Lepidocrocite
	Lepidocrocite	Ferric hydroxide

The products have been listed in order of increasing specific volume.
[a] May be from mill scale.

3.4. Mill-scale and corrosion

Mill-scale is the oxide film formed on the surface of rebar when it is hot rolled. Mill-scale on carbon steel is composed of wustite (FeO), magnetite (Fe_3O_4) and hæmatite (Fe_2O_3) [18]. The above oxides are formed in layers on the rebar surface, with wustite closest to the steel surface and hematite forming the outermost layer. In this project, magnetite and hæmatite were detected in the mill-scale by Raman spectroscopy; however, wustite was not observed probably because it did not exist in the region that was penetrated by the Raman laser.

The mill-scale on the rebar used in this project had a thickness of between 20 and 50 μm. EDS analysis of a cross-section of the as-received rebar (Fig. 12) revealed that mill-scale was primarily composed of iron and oxygen. The EDS analysis can only be considered as semi-quantitative and the lighter elements, such as oxygen, have a higher degree of uncertainty. However, based on a relative comparison

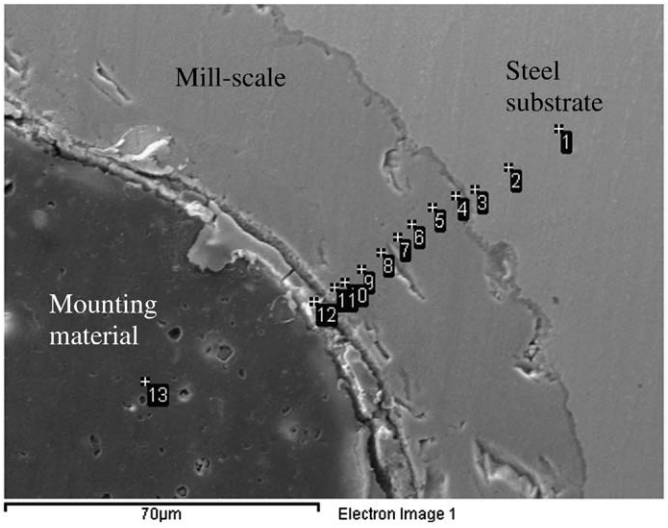

Spectrum	O	Si	Cl	Ca	Fe	Total
1	0.8	0.3	*0.0*	*0.0*	98.9	100.0
2	0.9	0.3	*0.1*	*0.0*	98.7	100.0
3	0.4	0.5	*-0.1*	*0.1*	99.1	100.0
4	12.7	0.8	*0.0*	*0.1*	86.4	100.0
5	12.9	*0.0*	*0.1*	*0.1*	86.9	100.0
6	13.3	*-0.2*	*0.0*	*0.0*	86.9	100.0
7	14.1	*-0.1*	*0.1*	*0.2*	85.7	100.0
8	13.4	*-0.1*	*-0.1*	*0.0*	86.8	100.0
9	14.6	*0.0*	*0.0*	*0.0*	85.4	100.0
10	16.5	*0.1*	*0.0*	*0.1*	83.3	100.0
11	16.6	*-0.1*	*0.1*	*0.2*	83.2	100.0
12	12.3	1.4	1.4	0.6	84.3	100.0
13	62.0	9.0	1.4	8.2	19.4	100.0

Fig. 12. SE image and EDS analysis (weight %) of a cross-section of rebar not embedded in concrete or exposed to chlorides. Numbers in italics are values below detectible limits.

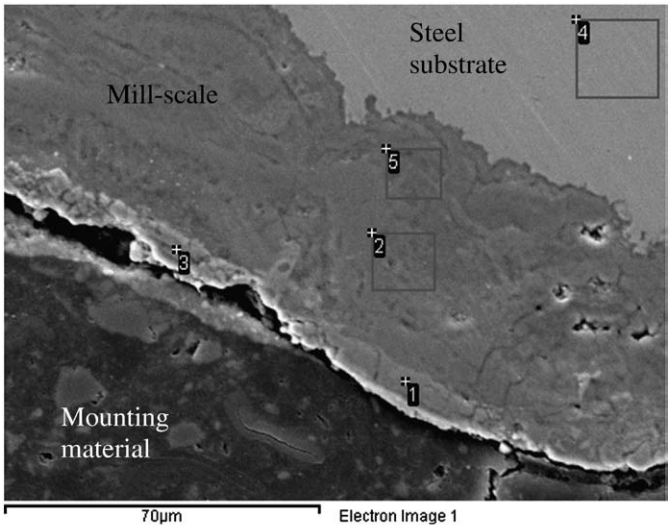

Spectrum	O	Si	Cl	Ca	Fe	Total
1	12.6	*0.1*	*0.0*	1.7	85.6	100.0
2	11.0	0.4	0.3	2.3	86.0	100.0
3	10.7	0.2	0.2	6.8	82.1	100.0
4	0.6	0.3	*0.1*	*0.1*	98.9	100.0
5	12.6	0.5	*0.1*	4.1	82.7	100.0

Fig. 13. SE image and EDS analysis (weight %) of a cross-section of rebar embedded in concrete but not exposed to chlorides. Numbers in italics are values below detectible limits.

of the data in Fig. 12, there was very little variation in iron and oxygen contents within the mill-scale. This could be because of the sample preparation technique which involved using water as the lubricant while grinding/polishing and exposing the sample to atmospheric conditions.

Calcium, silicon and chlorine contents in the mill-scale were also included in this analysis in order to determine the base amounts of these elements to enable comparison with analyses of rebar embedded in concrete and exposed to chlorides. The steel substrate contained a small amount of silicon. The mill-scale, on the other hand, had negligible amounts of calcium, silicon and chlorine. There was one spot (#12) on the rebar in Fig. 12 which had higher amounts of these elements than the rest of the sample. This spot was adjacent to the mounting material and (a) could have been contaminated by the mounting material during sample preparation or (b) EDS could have detected the mounting material together with the mill-scale.

EDS analysis on a sample of rebar embedded in sound OPCC that was not exposed to chlorides (here after called concrete bar) is shown in Fig. 13. The mill-scale of this bar appeared to be more porous/cracked and contained more calcium than that of the as-received bar. Typically, when surfaces are exposed to fresh concrete, calcium hydroxide precipitates on them [19]. However, because the mill-scale in the rebar was porous, calcium ions from the cement were able to penetrate into the mill-scale when it was embedded in fluid concrete. The calcium ions would have been accompanied by other ions (e.g. hydroxyl ions) which would allow products of cement hydration (e.g. calcium hydroxide) to form in the mill-scale. The formation of these hydration products could have induced further cracking in the mill-scale. The cracking could also have occurred when the rebar was removed from concrete.

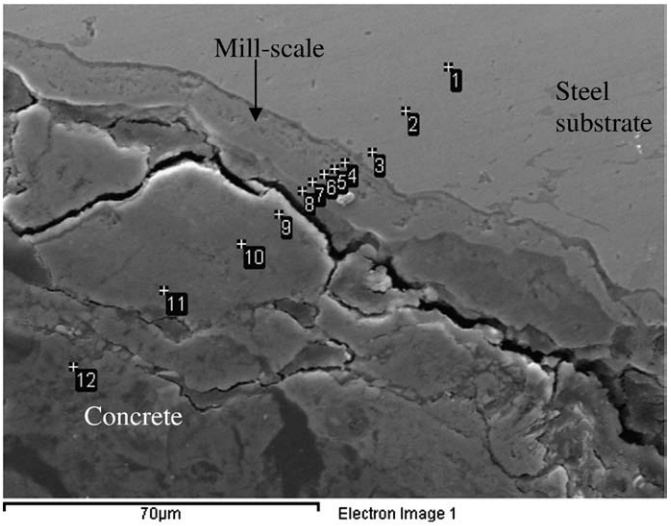

Spectrum	O	Si	Cl	Ca	Fe	Total
1	0.5	*0.1*	*0.1*	*0.1*	99.2	100.0
2	0.4	*0.1*	*0.1*	*0.0*	99.4	100.0
3	0.7	*0.1*	*0.0*	*0.2*	99.0	100.0
4	17.7	0.5	*0.1*	2.5	79.2	100.0
5	17.2	0.3	*0.1*	0.3	82.1	100.0
6	16.8	0.2	*0.1*	0.6	82.3	100.0
7	17.4	*0.1*	*0.0*	0.3	82.2	100.0
8	19.0	0.5	0.2	8.0	72.3	100.0
9	26.5	2.9	0.8	20.0	49.8	100.0
10	32.2	1.3	0.7	32.0	33.8	100.0
11	30.0	5.0	1.0	25.9	38.1	100.0
12	39.8	18.2	5.9	24.8	11.3	100.0

Fig. 14. SE image and EDS analysis (weight %) of mill-scale in the corroding bar. Numbers in italics are values below detectible limits.

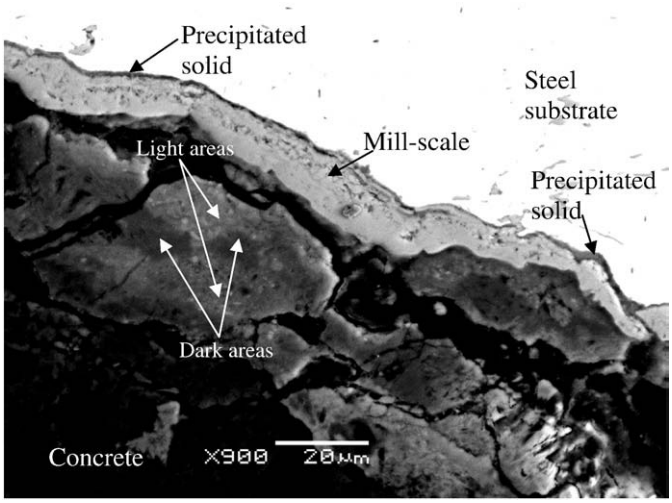

Fig. 15. A BSE image of the image shown in Fig. 14.

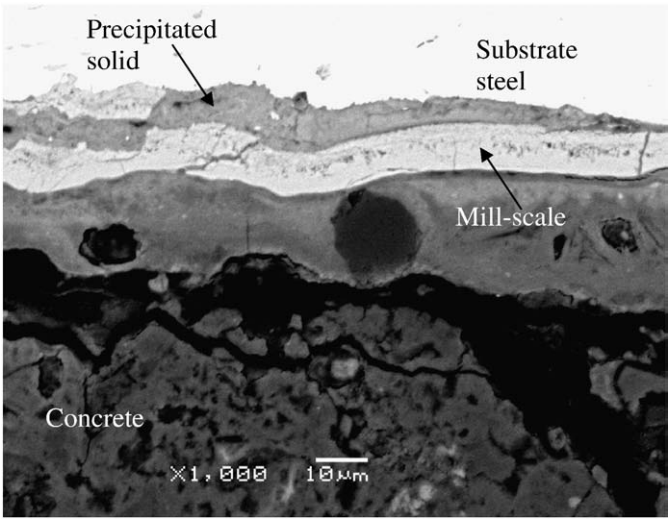

Fig. 17. A BSE image of the image shown in Fig. 16.

The silicon content was also higher in the mill-scale of the concrete bar than in the as-received bar. In Fig. 13, the silicon content decreased towards the surface of mill-scale, which could lead one to conclude that the steel substrate was the source of the silicon. However, this decrease was not observed in the other sections analysed. Hence, the source of silicon could also be the alite (C_3S) and belite (C_2S) phases in the cement. The mill-scale in the concrete bar contained lower amounts of silicon than calcium because (i) the cement components that react initially in water are tricalcium aluminate (C_3A) and gypsum ($C\bar{S}H_2$) [20] and (ii) unhydrated phases (except gypsum) contain more calcium than any other elements. The silicon and calcium could combine to form calcium-silicate-hydrate (C–S–H) in the mill-scale, which would also induce cracking in the mill-scale.

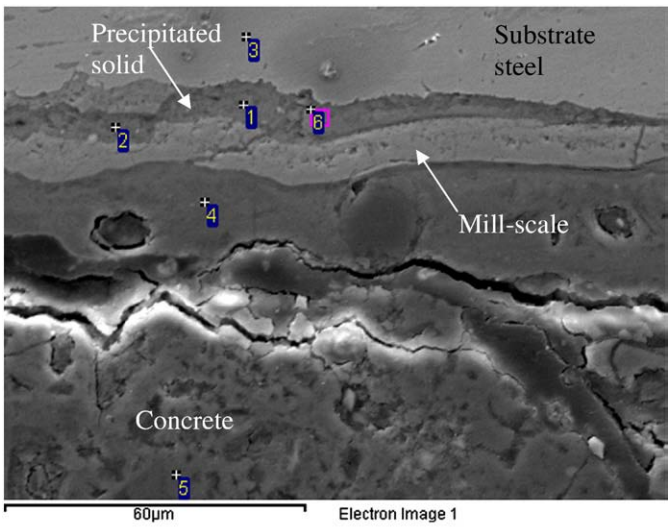

Spectrum	O	Si	Cl	Ca	Fe	Total
1	24.9	0.9	0.3	10.8	63.1	100.0
2	21.8	0.6	0.3	9.7	67.6	100.0
3	0.7	*0.2*	*0.2*	*0.2*	98.7	100.0
4	29.1	4.2	0.5	24.0	42.2	100.0
5	45.5	11.1	1.6	39.3	2.5	100.0
6	22.8	0.8	0.5	5.2	70.7	100.0

Fig. 16. SE image and EDS analysis (weight %) of precipitated solid. Numbers in italics are values below detectible limits.

The chloride content at two locations in Fig. 13 (# 2 and # 3) was higher than in the other locations. This locally high chloride content could be due to the contamination during sample preparation. Location # 3 was very close to the mounting material and could easily have been contaminated and location # 2 involved analysis of a large area that contained pores which could have trapped chlorides (e.g. from the mounting material).

Fig. 14 illustrates an EDS analysis of a cross-section of corroding rebar (corroding bar) from the cracked region of OPCC. A comparison of this analysis with that of the as-received bar showed the surface of the corroding bar was covered by a layer of mill-scale indicated by points # 4–# 7 in the SE image of Fig. 14. The silicon content of this mill-scale was similar to that observed in the mill-scale of the concrete bar; however, the calcium content was slightly lower. Points # 9–# 11 in Fig. 14 had high iron, calcium and silicon contents which implied that this region consisted of a combination of cement paste and corrosion products. This was confirmed by a BSE image (Fig. 15), which revealed a combination of light (high atomic weight elements e.g. Fe) and dark (low atomic weight elements e.g. Ca) areas in the region indicated by points # 9–# 11.

The BSE image clearly differentiates between the mill-scale and the corrosion products and shows a precipitated solid between the mill-scale and the substrate, in some areas. Under the BSE detection mode of the SEM, this solid has a similar colour to that of the cement paste/corrosion product combination (indicated by points # 9–# 11). The EDS analysis illustrated in Fig. 16 confirms the presence of calcium and iron in the precipitated solid implying that it is a mixture of paste and corrosion products. The corresponding BSE image is shown in Fig. 17. The exact mechanism of how this phase precipitated between the mill-scale and the substrate steel is unclear. However, the growth of this phase could have induced cracking in the mill-scale, thereby contributing to corrosion of the rebar.

4. Summary and conclusions

- Regardless of the type of loading, corrosion products on the rebar surface in OPCC were found in the vicinity of the intersecting concrete crack with an average spread along the bar of 40 mm. In HPC, the corresponding average spread was 75 mm. This difference was attributed to the lower porosity in HPC which prevented the diffusion of corrosion products into the adjacent concrete and confined them to the rebar–concrete interface. The implication of this build-up of corrosion products at the interface in HPC is that they could act as a wedge and result in spalling of large pieces of

concrete, which potentially catastrophic consequences. In OPCC, there is less likelihood of such spalling.

- In OPCC, corrosion products diffused from the crack into the aggregate–paste interface whereas they did not do so in the HPC. This indicates that the bond between the aggregates and cement paste in OPCC is more porous than in HPC. Also, more corrosion products were observed at the aggregate–paste interfaces in dynamically loaded OPCC than in statically loaded OPCC because (i) dynamic loading caused a greater detachment of bond between the aggregates and cement paste and (ii) the opening and closing of cracks in salt solution under dynamic loading forced corrosion products away from the rebar–concrete interface and into the crack.
- Corrosion products diffused from the cracks into the cement paste in dynamically loaded OPCC where they initiated cracking. This phenomenon was not observed in the statically loaded OPCC because there was a lower volume of corrosion products in the crack.
- Branched cracking observed in the dynamically loaded HPC was likely also caused by corrosion products.
- The most expansive corrosion product detected in the cracked concretes of this project was ferric hydroxide, with a specific volume four times larger than that of iron. This is the most voluminous corrosion product detected to date in reinforced concrete exposed to chlorides.
- The porous mill-scale on the surface of rebar allowed ions to ingress into it from the concrete and, possibly, to reach the reinforcing steel. This implies that the presence of mill-scale could delay the onset of corrosion on rebar; however, it does not prevent it.

Acknowledgements

The authors would like to thank the Natural Sciences and Engineering Research Council (NSERC) of Canada and the Cement Association of Canada for funding this project. The authors would also like to express their gratitude to Mr. Randal Fagan for instructions on using the Raman spectrometer. The help extended by Dr. Jeffrey S. West, Dr. Yuquan Ding, Messrs. John Boldt, Norval Wilhelm, Brad Bergsma, Kyle Anders, Ken Su and Ms. Katherine Olsen is greatly appreciated.

References

[1] T.D. Marcotte, Characterization of chloride-induced corrosion products that form in steel-reinforced cementitious materials, PhD Thesis in Mechanical Engineering. 2001, University of Waterloo: Waterloo, Canada.
[2] J.G. Cabrera, Deterioration of concrete due to reinforcement steel corrosion, Cement and Concrete Composites 18 (1) (1996) 47–59.
[3] C. Andrade, C. Alonso, F.J. Molina, Cover cracking as a function of bar corrosion: part I — experimental test, Materials and Structures 26 (8) (1993) 453–464.
[4] C.M. Hansson, Discussion of corrosion effects on bond strength in reinforced concrete. Paper by Kyle Stanish, R. D. Hooton, S. J. Pantazopoulou, ACI Structural Journal 97 (5) (2000) 789–790.
[5] A. Poursaee, C.M. Hansson, Potential pitfalls in assessing chloride-induced corrosion of steel in concrete. Cement and Concrete Research, submitted for publication.
[6] M.L. Allan, Probability of corrosion induced cracking in reinforced concrete, Cement and Concrete Research 25 (6) (1995) 1179–1190.
[7] A.K.M.F. Uddin, K. Numata, J. Shimasaki, M. Shigeishi, M. Ohtsu, Mechanisms of crack propagation due to corrosion of reinforcement in concrete by AE-SiGMA and BEM, Construction and Building Materials 18 (3) (2004) 181–188.
[8] M. Ohtsu, S. Yosimura, Analysis of crack propagation and crack initiation due to corrosion of reinforcement, Construction and Building Materials 11 (7–8) (1997) 437–442.
[9] S.J. Jaffer, C.M. Hansson, The influence of cracks on chloride-induced corrosion of steel in ordinary Portland cement and high performance concretes subjected to different loading conditions, Corrosion Science 50 (12) (2008) 3343–3355.
[10] K. Suzuki, Y. Ohno, S. Praparntanatorn, H. Tamura, Mechanism of steel corrosion in cracked concrete, International Symposium on Corrosion of Reinforcement in Concrete Construction (3rd), Elsevier Applied Science, Wishaw, England, 1990.
[11] K. Suda, S. Misra, K. Motohashi, Corrosion products of reinforcing bars embedded in concrete, Corrosion Science 35 (5–8) (1993) 1543–1549.
[12] K.K. Aligizaki, M.R. de Rooij, D.D. Macdonald, Analysis of iron oxides accumulating at the interface between aggregates and cement paste, Cement and Concrete Research 30 (12) (2000) 1941–1945.
[13] T.D. Marcotte, C.M. Hansson, The influence of silica fume on the corrosion resistance of steel in high performance concrete exposed to simulated seawater, Journal of Materials Science 38 (23) (2003) 4765–4776.
[14] T.D. Marcotte, C.M. Hansson, A comparison of the chloride-induced corrosion products from steel reinforced industrial standard versus high performance concrete exposed to simulated sea water, International Symposium on High-Performance and Reactive Powder Concretes, University of Sherbrooke, Sherbrooke, Québec, Canada, 1998.
[15] SSP 904 S13 High performance concrete, Ontario Provincial Standard Specification, 2005.
[16] S.J. Jaffer, The influence of loading on the corrosion of steel in cracked ordinary portland cement and high performance concretes, PhD Thesis in Mechanical Engineering. 2007, University of Waterloo: Waterloo, Canada.
[17] M. Odziemkowski, Email to S.J. Jaffer, 13th October 2007.
[18] D.C. Cook, Spectroscopic identification of protective and non-protective corrosion coatings on steel structures in marine environments, Corrosion Science 47 (10) (2005) 2550–2570.
[19] C.L. Page, Mechanism of corrosion protection in reinforced concrete marine structures, Nature 258 (1975) 514–515.
[20] K.L. Scrivener, The microstructure of concrete, in: J. Skalny (Ed.), Materials Science of Concrete, The American Ceramic Society, Westerville, OH, USA, 1989.